UDC 517.962: 517.968.2: 537.874.6: 621.391.1

L. A. Varianytsia-Roshchupkina, G. Gennarelli*, F. Soldovieri*, G. P. Pochanin
O. Ya. Usikov Institute for Radiophysics and Electronics of NAS of Ukraine
12, Ac. Proskura St., Kharkiv, 61085, *Ukraine*
E-mail: vla@ire.kharkov.ua; gpp@ire.kharkov.ua
**Institute for Electromagnetic Sensing of the Environment of CNR of Italy*
328,Via Diocleziano, Naples, 80124, Italy
E-mail: gennarelli.g@irea.cnr.it; soldovieri.f@irea.cnr.it

ANALYSIS OF THREE DIFFERENTIAL GPR SYSTEMS FOR SUBSURFACE IMAGING

Quality of the radar images of the detected objects directly depends on the quality of the obtained GPR data. One of the ways to increase the information content of such data is to use not traditional (monostatic, bistatic) but alternative (e. g., differential) antenna systems. The goal of this work is to analyze and compare possibilities of imaging using differential antenna systems with receiving antennas displaced symmetrically with respect to the transmitting antenna along three orthogonal directions. To this end, synthetic radargrams are generated by the finite-difference time-domain forward solver for each measurement setup. After that a microwave tomographic approach is applied to process the scattered field differential data and to facilitate the comparison among these systems. As a result, it was obtained that the system with antennas displaced along the vertical axis is the only one capable to provide a reliable image regardless of the shape of the object. The performed studies have shown the prospects of such system application in the practical GPR problems. Fig. 14. Table 1. Ref.: 19 titles.

Key words: GPR, differential antenna systems, FDTD, microwave tomography.

The choice of the optimal Ground Penetrating Radar (GPR) system configuration is a crucial factor for the imaging capabilities of subsurface radar [1, 2]. The bistatic antenna system with a common-offset transmitter and receiver pair is the most commonly adopted solution for a modern GPR. The main drawback of such system is that the signal collected by the receiver (total signal) includes not only a signal scattered from the object, but also the direct signal from the transmitter to the receiver (which does not convey any information about the target). Usually, the amplitude of the direct signal is much larger than that reflected by the object. It complicates the target detection. In addition, this coupling limits the dynamic range of the GPR, and powerful direct signal may damage a sensitive input circuit of the receiver.

In order to eliminate the incident field from the total field signal, the multi-bistatic differential systems were suggested in [3–7]. The basic principle of differential systems is in the use of central symmetry in configurations like transmitter – receiver – transmitter (TRT) or receiver – transmitter – receiver (RTR). The couplings of two transmitters in the TRT-system cancel each other at the receiver. For the RTR-system, the direct signal from the transmitter is canceled at two receivers by subtraction of the total signals.

In the case of a differential system with horizontal spacing between the antennas, if the ground is homogeneous and all interfaces are uniform, the signals reflected by the interfaces are also canceled out at the input of receiver.

Theoretical studies in papers [3–7] have shown a high efficiency of the application of differential antenna systems for GPR investigations. However, the practical implementation of the proposed ideas is complicated by the difficulties of creation of the geometrically and physically completely symmetric system. A slightest inaccuracy in the construction or discrepancy in characteristics of pairs of components can have a catastrophic impact on the performance of the whole system. So, the difficulties associated with practical implementation of the system limit the possibility of its application for real GPR problems solving.

One of the earliest real developments of the differential antenna system with horizontally separated antennas is described in [8]. As previously noted, such system could be useful for the detection of localized buried targets. However, such systems are unsuitable for detecting the extended buried targets like layers. Accordingly, a differential system with vertically spaced antennas was suggested in [9–11]. In [8–11] it was proposed to subtract signals coming from two receiving antennas in the summator. It allowed getting zero direct coupling signal at the input of the receiver. In practice, such antenna system (GPR “ODYAG”) made it possible to reach the decoupling level of about –100 dB [10].

The preliminary theoretical comparisons of imaging possibilities of the horizontal and vertical differential systems were recently carried out in case of the conducting objects located in a 2D free space scenario [12]. In particular, it was shown that a more reliable image of the object can be generally obtained by using the receiving antennas displaced vertically. In case of horizontally spaced receivers only edges of targets can be imaged.

The aim of this work is to extend the previous analysis to the 3D-geometry in the case of conductive and dielectric objects. We consider the sounding of different geometrical structures by three differential GPR systems (Fig. 1) and compare their imaging performance. Synthetic scattered field data are generated by means of an ad-hoc developed Finite-Difference Time-Domain (FDTD) code [13]. In

addition, in order to improve the interpretation of the results with respect to radargrams, the data are processed by means of the microwave tomographic approach similar to the one reported in [7] for the 2D case. Reconstruction results are shown to support the analysis and compare the systems.

1. Problem statement. For the sake of simplicity, we consider the 3D free-space scenario depicted in Fig. 1, a. A target Q stands in the investigation domain D, and the scene is probed by an antenna system moving on the survey plane Γ at $z = 0$ under a reflection configuration. The distance between the nearest edge of the object Q and the survey plane Γ is denoted as h.

Fig. 1, b depicts three differential antenna systems consisting of the transmitting antenna T and a pair of receiving antennas R symmetrically spaced with respect to T along x, y or z at distance h_s. We denote each system using the following notation: ($R_{x-}\, T\, R_{x+}$) and ($R_{y-}\, T\, R_{y+}$) are "horizontal" Systems I and II respectively, ($R_{z-}\, T\, R_{z+}$) is a "vertical" System III. Each antenna is simulated here as a Hertzian dipole directed along the y-axis. These three antenna systems move simultaneously along survey lines in Γ-plane parallel to the x-axis at different values of the y_0 coordinate.

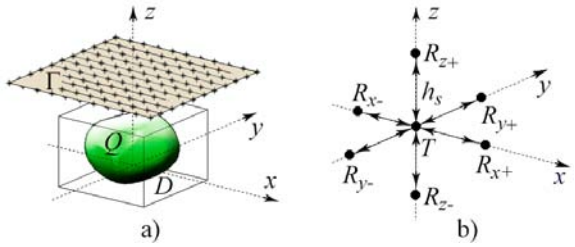

Fig. 1. Geometry of the imaging problem

The transmitting dipole is excited by the current pulse $I(t)$ with temporal variation corresponding to the time derivative of Gaussian pulse (Ricker function):

$$I(t) = -2\varsigma e^{1/(4\varsigma)}(t-\delta)\exp\left(-\varsigma(t-\delta)^2\right), \qquad (1)$$

where $\varsigma = 2\pi^2 f^2$ and $\delta = 1/f$, with f being the central frequency of the pulse.

In this work, we focus on imaging three types of objects. The first one is a rectangular bar with sizes $l_x \times l_y \times l_z$, the second one is a sphere of radius l and the last one is a combination of two rectangular bars with sizes $l_x^1 \times l_y^1 \times l_z^1$ and $l_x^2 \times l_y^2 \times l_z^2$ spaced by distance h_1 (Fig. 2). For the bar, both cases of dielectric (relative permittivity $\varepsilon = 1.3$) and perfectly conducting targets will be addressed; while only metallic sphere and metallic combined target are considered.

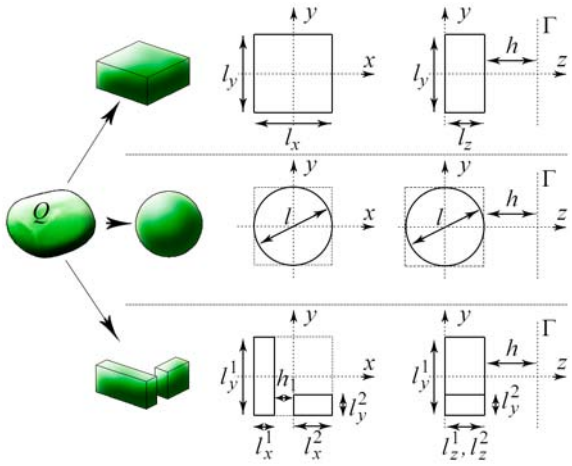

Fig. 2. Geometry of the targets Q

These types of object have been selected in order to evaluate the systems' performance for both the localized and elongated targets.

2. Microwave tomographic approach. In this section, we describe the inversion approach used to retrieve the object profile from the scattered field data.

We denote with $\vec{r}_0 = (x_0, y_0, 0)$ the coordinates of the transmitting antenna T. Moreover, $\vec{r}_{x\mp} = (x_0 \mp h_s, y_0, 0)$, $\vec{r}_{y\mp} = (x_0, y_0 \mp h_s, 0)$, and $\vec{r}_{z\mp} = (x_0, y_0, \mp h_s)$ are the positions of the receivers in Systems I, II, III, respectively.

The data to be inverted are the difference of total fields measured by receivers while the antennas move along Γ. To simplify the problem, we adopt a linearized inverse scattering model based on the Born approximation [7, 14, 15]. Accordingly, the functional relationships between the frequency domain data and the target in D are linear. In particular, we have:

$$\Delta E_y^I(\vec{r}_0, f) = E_y^{tot}(\vec{r}_{x-}, f) - E_y^{tot}(\vec{r}_{x+}, f) = \\ = k_0^2 \iiint_D \left[G(\vec{r}_{x-}, \vec{r}', f) - G(\vec{r}_{x+}, \vec{r}', f) \right] \times \vec{E}^{inc}(\vec{r}_0, \vec{r}', f)\chi(\vec{r}')d\vec{r}' \times \vec{e}_y \qquad (2)$$

for System I. In eq. (2), f is the work frequency, E_y^{tot} is the y-component of the total field at the receivers R_{x-}, R_{x+}; k_0 is wave number of free-space; G is the dyadic Green's function in free-space [16]; $\vec{E}^{inc}$ is the incident field at the point $\vec{r}' = (x', y', z')$ in D; and $\chi = \varepsilon - 1$ is the unknown object contrast, where ε is a relative permittivity of the object; $d\vec{r}' = dx'dy'dz'$; $\vec{e}_y = (0,1,0)$ is the y-directed unit vector. Functional relationships for $\Delta E_y^{II}(\vec{r}_0, f)$ and $\Delta E_y^{III}(\vec{r}_0, f)$ relevant to Systems II and III can be written in a similar way.

Once the differential scattered field data $\Delta E_y^{\mathrm{I,II,III}}$ have been gathered, the imaging problem amounts to performing the inversion of the corresponding linear operators with respect to the unknown χ. Such a problem is ill-posed and a regularized solution is obtained by applying the Truncated Singular Value Decomposition (TSVD) algorithm [17]:

$$\chi(x',z') = \sum_{n=0}^{N} \frac{\langle \Delta E_y, v_n \rangle}{\sigma_n} u_n, \qquad (3)$$

where N_T is a truncation index determining the "degree of regularization" of the solution, $\langle \cdot,\cdot \rangle$ denotes a scalar product, $\{\sigma_n\}_{n=0}^{\infty}$ is a set of singular values in non-increasing order, $\{v_n\}_{n=0}^{\infty}$ and $\{u_n\}_{n=0}^{\infty}$ are basis functions in the data and unknown spaces, respectively [17].

3. Numerical simulation. The radar signals are computed by an ad-hoc developed 3D-code [13] based on the FDTD-method. Perfectly absorbing boundary conditions [18] are used in order to limit the computational domain. Image profiles (B-scans) are obtained by the program "GPR ProView" of GPR data processing [19]. These program modules have been developed and implemented in O. Ya. Usikov Institute for Radiophysics and Electronics of NAS of Ukraine. The method of variable density [1] is used for result visualization.

For the simulations, we choose the following input parameters:

– source T is located at the distance $h = 0.3$ m from the object;

– distance h_s between T and the receivers is fixed to 0.05 m;

– central frequency of the pulse $f = 1$ GHz;

– object sizes are $l_x = l_y = 2l_z = 0.4$ m; $l = 0.1$ m and $l_y^1 = 2l_z^1 = 4l_x^1 = 0.4$ m and $l_x^2 = 2l_y^2 = l_z^2 = 0.2$ m; the distance h_1 between the objects in pair is 0.1 m.

Other parameters related to the problem are listed in the Table below.

Simulation parameters

Parameter	Value
Size of the measurement domain Γ	1×1 m^2
Transmitter measurement step	0.1 m
Number of measurement points	11×11
Time window for each trace	8 ns
Number of time samples for each trace	416

3.1. Synthetic radargrams. The radargrams corresponding to the dielectric and conducting bars are shown in Fig. 3 and 4 for different antenna systems and two survey lines. The same is done for the conducting sphere and two conducting bars in Fig. 5 and 6.

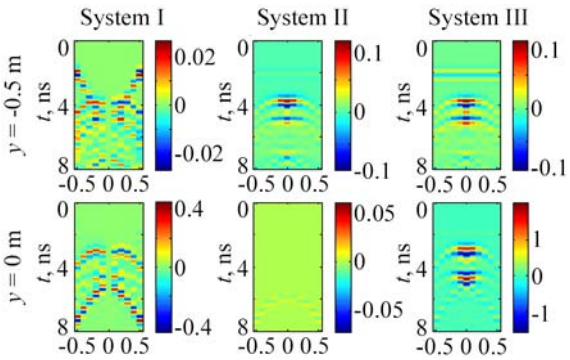

Fig. 3. Radargrams of the dielectric bar

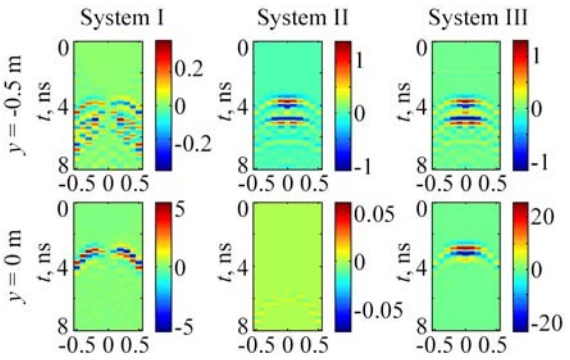

Fig. 4. Radargrams of the conducting bar

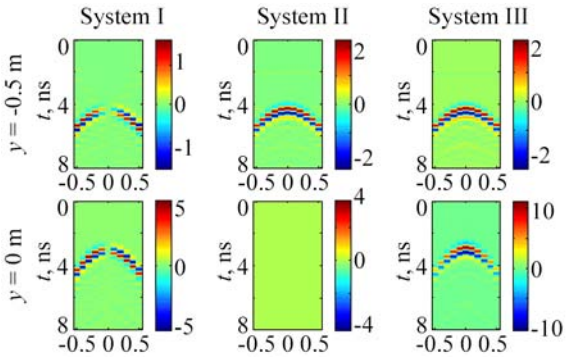

Fig. 5. Radargrams of the conducting sphere

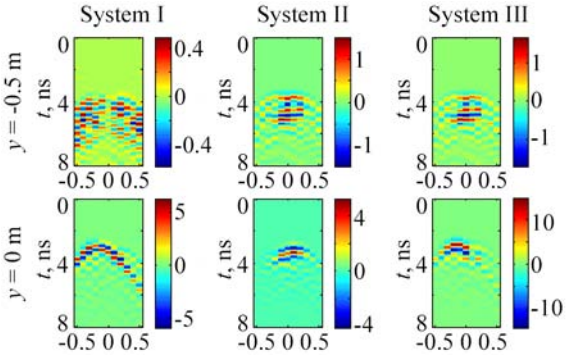

Fig. 6. Radargrams of a pair of conducting bars

From the analysis of radargrams, it is possible to make some common conclusions:

– When using Systems I, II and III instead of the traditional multi-bistatic configuration, the radargrams contain only the signals scattered by the objects. In this way, the object detection is possible without any additional processing. A quite different situation occurs when the survey line is in the plane of object symmetry and receiving antennas are symmetrical to this plane; in this case, no object response is observed in the radargram (the case of System II with $y = 0$ in Fig. 3–5).

– Because of the symmetry problem, the System I cannot image the middle part of the object.

– In case of the antenna system moving on the bottom edge of the survey plane ($y = –0.5$), the position and geometrical characteristics of the reflecting object are similar for System II and System III. The existing difference in extension of reflecting surfaces has only a minor influence on the image of the object in radargram and is almost undistinguished by eye (see Fig. 3–6).

The analysis of radargams of dielectric and conducting bars shows that the presence of the rectangular bar in radargram can be detected by local horizontal fascias when using Systems II and III, and by sections of hyperbolic curves that indicate edges of the bar when using System I.

In both cases (dielectric and conducting objects), radargrams corresponding to the bottom edge of the survey plane ($y = –0.5$) provide information about both front and back sides of bars. While the central location of the antenna system survey line ($y = 0$) provides information about both front and back sides of bars in case of the dielectric object only (Except for System II). In this case we can detect only the front side of the conducting object.

In case of the dielectric object, spurious reflections from the absorbing boundary conditions (see Fig. 3, oblique line segments in the time interval [2, 4] ns at $y = –0.5$ m and [5, 8] ns at $y = 0$ m), are more significant.

We can note that the signals of maximal amplitude are observed in System III when the antenna system is placed over the center of the target. When the antenna System II is placed over the center of the target, the reflected signal is of zero amplitude.

The radargrams corresponding to conducting objects of different geometrical shapes are shown in Fig. 4–6 for different antenna systems and survey lines. We can state that:

– The spherical object in the radar image is represented as a hyperbolic curve (for all types of antenna systems).

– Two bars in the radar image are represented as a series of hyperbolic curves (for all types of antenna systems). And it can be noticed that at the central location of the antenna system survey line ($y = 0$) different antenna systems detect objects in a different way: System I detects one object, System II detects another one, and System III combines information about both of them.

– Representations of objects of different geometrical forms are very much similar for System I (they are always hyperbolic curves) and they can be different for System II and System III. But in any case it is difficult to recognize the object geometry without additional processing (especially in case of two closely spaced objects, see Fig. 6).

3.2. Tomographic reconstruction. The time domain scattered field data collected under configurations I, II and III have been processed through the tomographic approach. The corresponding software is developed and implemented in the Institute for Electromagnetic Sensing of the Environment of CNR of Italy.

The working frequency band [500, 2 000] MHz is considered and sampled with a step of 250 MHz. The targets are centered in the investigation domain $D = [–0.4,\ 0.4]\times[–0.4,\ 0.4]\times[0.2,\ 0.6]$ m^3, which is discretized into voxels with size $\Delta x = \Delta y = 0.05$ m and $\Delta x = 0.025$ m. The truncation index of the TSVD inversion scheme in (3) is selected in a way to filter singular values that are 25 dB lower than the maximum one.

The tomographic images of different objects are shown in Fig. 7–14.

Dielectric and conducting bars. The tomographic images shown in Fig. 7 and 8 refer to the dielectric bar.

It can be seen that System I allows detecting the edges aligned with the *y*-axis. System II permits to identify the edges directed along the *x*-axis. System III allows reconstructing the full geometry of both the upper and lower surface of the object. Therefore, System III allows getting clearer image of the object and identifying better its shape.

As expected, the same considerations hold for the metallic bar (Fig. 9 and 10), except for the fact that now it is impossible to get information about the lower surface because of full reflection by the upper and lateral sides of the object.

Conducting sphere. The results of microwave tomographic reconstruction for this kind of target are presented in Fig. 11 and 12.

For System I, the tomographic image of the spherical object is three elliptic objects elongated in *y*-direction and spaced in *x*-direction. For System II, the tomographic image of the spherical object is three elliptic objects elongated in *x*-direction and spaced in *y*-direction. System III allows getting a clearer image of the object and to identify better its spherical shape.

Two conducting bars. Resolution and detection of closely set targets is one of the important problems of modern GPR. In Fig. 13 and 14, the tomographic images of such kind of targets (two conducting bars) are presented.

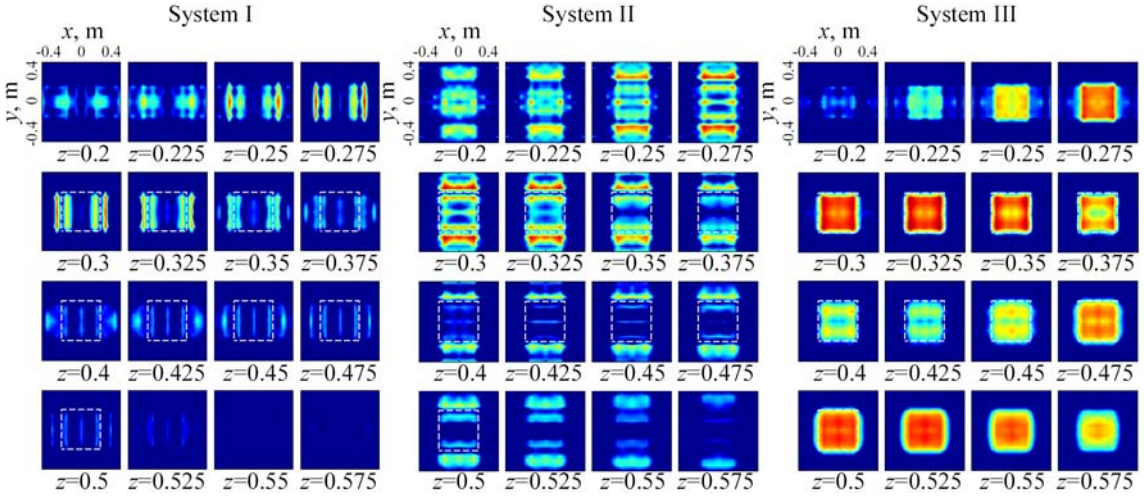

Fig. 7. Z-slices of the tomographic reconstruction of the dielectric bar

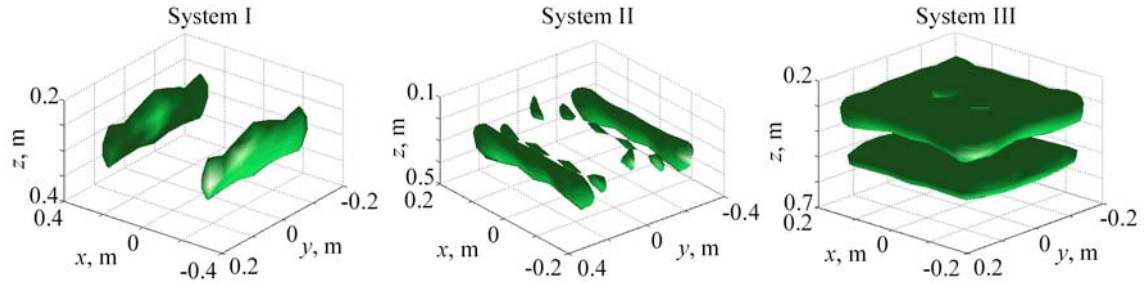

Fig. 8. Isosurface plot of the tomographic reconstruction of the dielectric bar

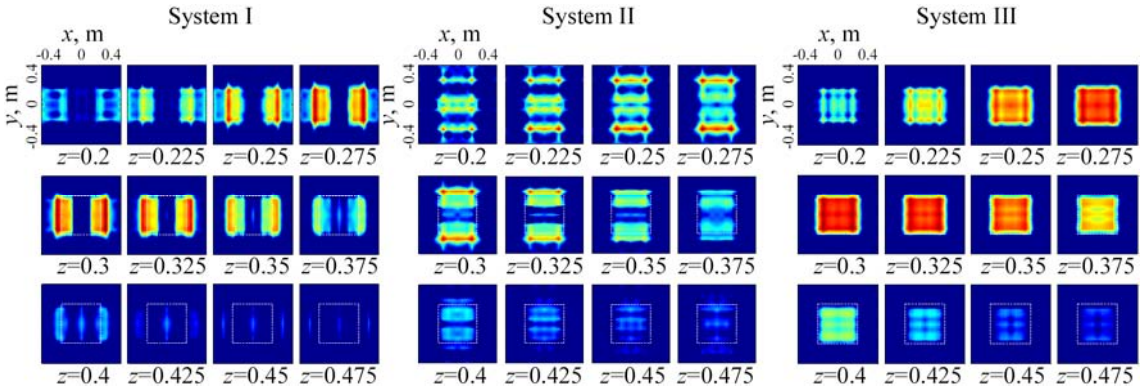

Fig. 9. Z-slices of the tomographic reconstruction of the metallic bar

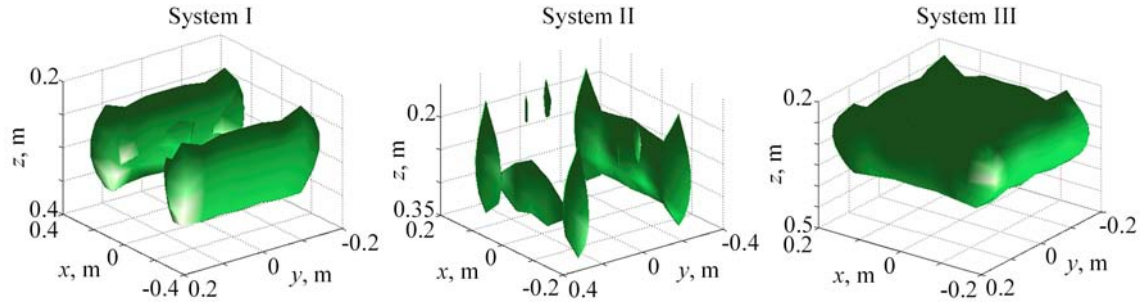

Fig. 10. Isosurface plot of the tomographic reconstruction of the metallic bar

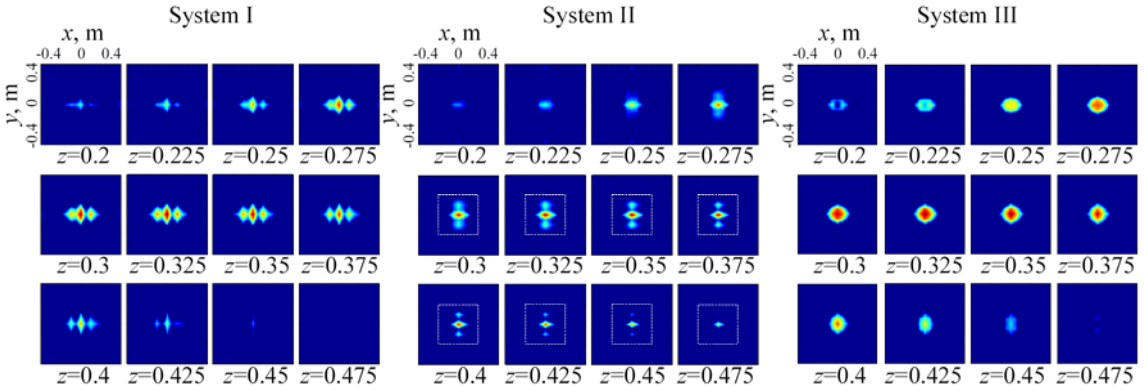

Fig. 11. Z-slices of the tomographic reconstruction of the metallic sphere

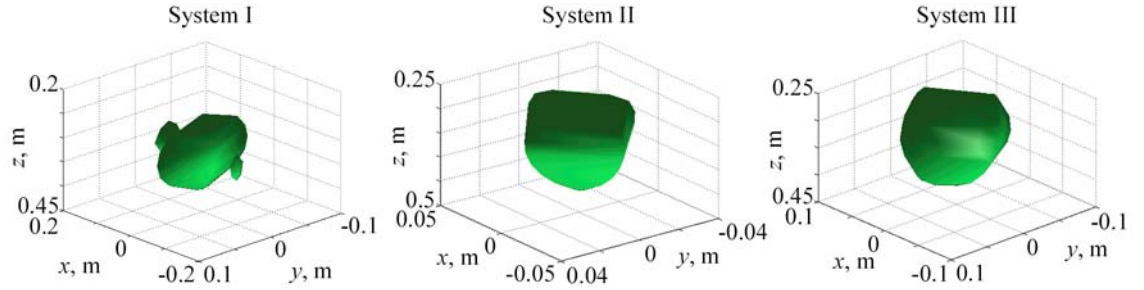

Fig. 12. Isosurface plot of the tomographic reconstruction of the metallic sphere

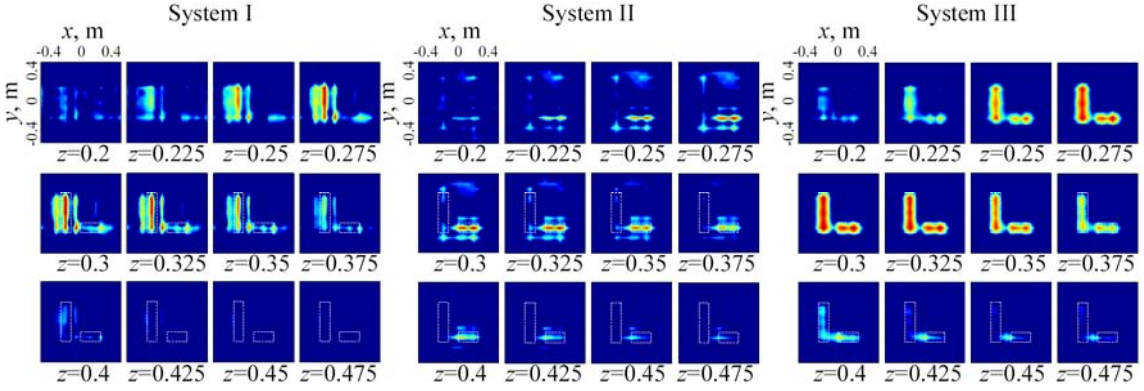

Fig. 13. Z-slices of the tomographic reconstruction of a pair of metallic bars

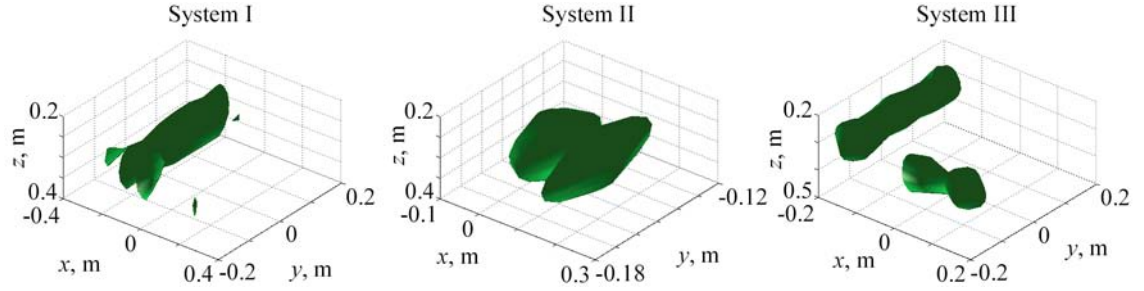

Fig. 14. Isosurface plot of the tomographic reconstruction of a pair of metallic bars

We can state that it is very difficult to detect the presence of the second ("*x*-oriented") object for System I. For System II, it is almost impossible to detect the presence of the first ("*y*-oriented") object.

In order to detect these low contrast objects the threshold value has to be fixed at a quite low value, which is comparable with the level of noise.

But System III similarly to previous cases gives us a quite clear image of the objects and allows identifying its shape.

Conclusions. In this work, we have compared the capabilities of three differential GPR systems with symmetrical receiving antennas displaced along three orthogonal directions with respect to the transmitting antenna. Synthetic radar images have been computed and analyzed.

It has been shown:

– When using Systems I, II and III instead of the traditional multi-bistatic configuration, the object detection is possible without any additional processing, because the radargrams do not contain masking high power signals of direct coupling. Except for the situation when the survey line is in the plane of the object symmetry and receiving antennas are placed symmetrically to this plane. In this case the object becomes “invisible”.

– Objects of different geometrical shapes can have different representations in radargrams (fascia, hyperbolic curve). But in any case, it is difficult to identify their geometries without additional processing (especially in case of two closely spaced objects).

The microwave tomographic approach has proved to be a valuable tool to support the proposed analysis. Indeed, it has been shown:

– In case of one rectangular bar, the target form can be recovered, despite the fact that each system can only provide information about a pair of object surfaces. But the correct information about object dimensions can be obtained for the dielectric bar only, when using System III. For metal objects, size measurement is possible for only two of three coordinate directions (length, width, but not depth).

– For GPR investigations of such objects as a sphere and especially a pair of bars, using the differential systems with receivers lying in the measurement plane leads to the loss of the information about the shape and size of target. The vertical spacing of receiving antennas allows getting more reliable images of objects in such problems.

Thus, the analysis has revealed the advantages of using a differential antenna system with vertically spaced different antennas for reconstructing the shape and dimensions of sounding objects in free space. Thereby the performed studies have shown that the application of such systems in the practical GPR problems is very promising.

The research has been performed in the framework of the Active and Passive Microwaves for Security and Subsurface imaging (AMISS) EU 7th Framework Marie Curie Actions IRSES project (PIRSES-GA-2010-269157).

References

1. *Vladov M. L.* Introduction to GPR: Tutorial (in Russian) / M. L. Vladov , A. V. Starovoytov. – M.: Moscow University Press, 2004. – 153 p.
2. *Grinev Yu.* Problems of subsurface radiolocation (in Russian) / Yu. Grinev. – M.: Radiotechnics Press, 2005. – 416 p.
3. *Curtin R. B.* Technique for Measuring Electric Field Signals Using a Differential Antenna system / R. B. Curtin // IEEE Trans. Electrom. Compatibility. – 1967. – 9, N 1. – P. 24–25.
4. *Luneau P.* Underground target probing using FDTD / P. Luneau, G. Y. Delisle // IEEE AP-S Intern. Symp. and URSI Radio Science Meeting: proc. – Baltimore, Maryland, 1996. – P. 1664–1667.
5. *Gurel L.* Three-Dimensional FDTD modeling of a ground penetrating radar / L. Gurel, U. Oguz // IEEE Trans. Geosci. Remote Sensing. – 2000. – 38, N 4. – P. 1513–1521.
6. *Palmer K. D.* Differential antenna feeding system for short range UWB radar / K. D. Palmer, J. H. Zijderveld, A. G. Yarovoy // First European Radar Conference (EURAD 2004): proc. – Amsterdam, 2004. – P. 21–24.
7. *Persico R.* A microwave tomography approach for a differential configuration in GPR prospecting / R. Persico, F. Soldovieri // IEEE Trans. Antennas Propag. – 2006. – 54, N 11. – P. 3541–3548.
8. *The* use of the monopulse type antenna system in GPR for increasing accuracy of horizontal coordinate measurement / G. P. Pochanin, Yu. A. Kopylov, A. A. Orlenko, P. V. Kholod // The Second Intern. Workshop “Ultra Wideband and Ultra Short Impulse Signals” (UWBUSIS 2004): proc. – Sevastopol, 2004. – P. 217–219.
9. *Patent* 81652 Ukraine, IPK H 01 Q 9/00, H 01 Q 19/10. The method of recoupling between transmitting and receiving modules of the antenna system (in Ukrainian) / Yu. O. Kopylov, S. O. Masalov, G. P. Pochanin; applicant and patentee IRE of NAS of Ukraine. – № a2005 08109; filed 17.08.05; issued 25.01.08, Bull. №2. – 7 p.
10. *Pochanin G. P.* High decoupled antenna for UWB pulse GPR “ODYAG” / G. P. Pochanin, A. A. Orlenko // 4th Intern. Workshop “Ultra Wideband and Ultra Short Impulse Signals” (UWBUSIS 2008): proc. – Sevastopol, 2008. – P. 163–165.
11. *Measuring* of Thickness of the Asphalt Pavement with Use of GPR / G. P. Pochanin, V. P. Ruban, A. G. Batrakova et al. // 15th Intern. Radar Symp.: proc. – Gdansk, 2014. – P. 452–455.
12. *Varyanitza-Roshchupkina L. A.* Comparison of Two Differential GPR systems for Imaging Objects under a Reflection Configuration / L. A. Varyanitza-Roshchupkina, G. Gennarelli, F. Soldovieri // 15th Intern. Radar Symp.: proc. – Gdansk, 2014. – P. 435–438.
13. *Varyanitza-Roshchupkina L. A.* Software for image simulation in ground penetrating radar problems / L. A. Varyanitza-Roshchupkina // III Intern. Workshop “Ultra Wideband and Ultra Short Impulse Signals” (UWBUSIS 2006): proc. – Sevastopol, 2006. – P. 150–155.
14. *Gennarelli G.* A linear inverse scattering algorithm for radar imaging in multi-path environments / G. Gennarelli and F. Soldovieri // IEEE Geosci. Remote Sens. Let. – 2013. – 10, N 5. – P. 1085–1089.
15. *Persico R.* A Microwave Tomographic Imaging Approach for Multibistatic Configuration: The Choice of the Frequency Step / R. Persico, F. Soldovieri, G. Leone // IEEE Trans. Instrumentation and Measurement. – 2006. – 55, N 6. – P. 1926–1934.
16. *Balanis C. A.* Antenna Theory: Analysis and Design / C. A. Balanis. – N. Y.: Wiley, 2012. – 1136 p.
17. *Bertero M.* Introduction to Inverse Problems in Imaging / M. Bertero, P. Boccacci. – Bristol, U. K.: Inst. Phys. CRC Press, 1998. – 352 p.
18. *Sirenko Yu. K.* Simulation and analysis of transient processes in open periodic, waveguide and compact resonators (in Russian) / Yu. K. Sirenko. – Kharkov: Edena, 2003. – 363 p.
19. *Golovko M. M.* Representation of the Results of Subsurface Videopulse Sounding (in Russian) / M. M. Golovko,

G. P. Pochanin, V. O. Kovalenko // Radiophysics and electronics: proc. / Institute for Radiophysics and Electronics of NAS of Ukraine. – Kharkov, 2000. – 5, N 2. – P. 134–143.

Рукопись поступила 21.11.2014.

Л. А. Варяница-Рощупкина, Дж. Дженнарелли,
Ф. Сольдовьери, Г. П. Почанин

АНАЛИЗ ТРЕХ ДИФФЕРЕНЦИАЛЬНЫХ КОНФИГУРАЦИЙ ГЕОРАДАРОВ С ТОЧКИ ЗРЕНИЯ КАЧЕСТВА ОТОБРАЖЕНИЯ ПОДПОВЕРХНОСТНЫХ ОБЪЕКТОВ

Качество радиолокационных изображений обнаруживаемых объектов напрямую зависит от качества получаемых георадиолокационных данных. Одним из путей повышения информативности таких данных является использование не традиционных (моностатической, бистатической), а альтернативных (к примеру, дифференциальных) антенных систем. Цель работы состоит в том, чтобы проанализировать и сравнить визуализационные возможности дифференциальных конфигураций антенных систем, составленных из приемной антенны – передающей антенны – приемной антенны, в которых приемные антенны симметрично смещены относительно передающей антенны вдоль трех ортогональных направлений. Для этого выполнено *FDTD*-моделирование радарограмм для каждой измерительной конфигурации. Для обработки дифференциальных данных полей рассеяния и сравнения между системами использован метод микроволновой томографии. Установлено, что только система с вертикально разнесенными антеннами способна обеспечить наиболее реалистичное изображение независимо от формы исследуемого объекта. Проведенные исследования показали перспективность применения такой системы в практических задачах георадиолокационного зондирования.

Ключевые слова: *GPR*, дифференциальная антенная система, *FDTD*, микроволновая томография.

Л. А. Варяниця-Рощупкіна, Дж. Дженнареллі,
Ф. Сольдов’єрі, Г. П. Почанін

АНАЛІЗ ТРЬОХ ДИФЕРЕНЦІЙНИХ КОНФІГУРАЦІЙ ГЕОРАДАРІВ ВІДНОСНО ЯКОСТІ ВІДОБРАЖЕННЯ ПІДПОВЕРХНЕВИХ ОБ’ЄКТІВ

Якість радіолокаційних зображень об’єктів, що треба виявити, безпосередньо залежить від якості одержуваних георадіолокаційних даних. Одним із шляхів підвищення інформативності таких даних є використання не традиційних (моностатичної, бістатичної), а альтернативних (наприклад, диференційних) антенних систем. Мета роботи полягає у тому, щоб проаналізувати й порівняти візуалізаційні можливості диференційних конфігурацій антенних систем, що складаються з приймальної антени – передавальної антени – приймальної антени, у яких приймальні антени симетрично зміщені відносно передавальної антени вздовж трьох ортогональних напрямків. Для цього виконано *FDTD*-моделювання радарограмм для кожної вимірювальної конфігурації. Для обробки диференційних даних полів розсіювання та порівняння між системами використано метод мікрохвильової томографії. Встановлено, що тільки система з вертикально рознесеними антенами здатна забезпечити найбільш реалістичне зображення незалежно від форми досліджуваного об’єкта. Проведені дослідження показали перспективність застосування такої системи в практичних задачах георадіолокаційного зондування.

Ключові слова: *GPR*, диференційна антенна система, *FDTD*, мікрохвильова томографія.